01 Nov 2023

Effect Of Type And Quantity Of Inherent Alkali Cations On Alkali-silica Reaction

Pengfei Ma

Jiaoli Li

Jincheng Bai

Ying Zhuo

et. al. For a complete list of authors, see https://scholarsmine.mst.edu/civarc_enveng_facwork/2610

Recommended Citation

P. Ma et al., "Effect Of Type And Quantity Of Inherent Alkali Cations On Alkali-silica Reaction," *Cement and Concrete Research*, vol. 173, article no. 107293, Elsevier, Nov 2023.
The definitive version is available at https://doi.org/10.1016/j.cemconres.2023.107293

Cement and Concrete Research 173 (2023) 107293

Contents lists available at ScienceDirect

Cement and Concrete Research

journal homepage: www.elsevier.com/locate/cemconres

Effect of type and quantity of inherent alkali cations on alkali-silica reaction

Pengfei Ma [a], Jiaoli Li [a], Jincheng Bai [b], Ying Zhuo [a], Lingyu Chi [c], Yanping Zhu [a], Zhenhua Shi [a], Hongyan Ma [a], Genda Chen [a,*]

[a] Department of Civil, Architectural and Environmental Engineering, Missouri University of Science and Technology, Rolla, MO, USA
[b] Materials Research Center, Missouri University of Science and Technology, Rolla, MO, USA
[c] Department of Chemistry, Missouri University of Science and Technology, Rolla, MO, USA

ARTICLE INFO

Keywords:
Alkali-silica reaction
Sodium and potassium
Boosting and exposing
Raman spectroscopy
Expansion mechanism

ABSTRACT

In this study, the macroscopical expansion induced by alkali-silica reaction (ASR) and its corresponding ASR products are investigated using ordinary Portland cement (OPC) mortar specimens with a gradient of boosted alkalis. Experimental results show that the expansion increases with the concentration of inherent alkalis. Sodium-boosted samples expand approximately three times as much as potassium-boosted samples. ASR gels that are present in aggregate veins are calcium-free and amorphous; the atomic ratios of ASR gels are nearly independent of the type and quantity of alkali cations. Aggregate ASR gel exudation occurs in high (≥2.5 %) sodium cases and produces potential Na-shlykovite. Crystalline and amorphous calcium-containing ASR products are present in aggregate vicinities in either Na- or K-boosted samples. The higher hydrophilicity of Na-gel in aggregate veins accounts for the larger expansion. Boosted alkali cations are more effective in ASR products formation than in exposing solution. A new observation that NaOH exposure inhibits ASR in K-boosted samples (zero expansion) is reported.

1. Introduction

Alkali-silica reaction (ASR), in juxtaposition of carbonization [1], chloride penetration [2], and sulfate attack [3], causes deteriorations of concrete structures [4–6]. The reaction is initiated by the assault of hydroxyl groups on the metastable silicate phases in reactive aggregates [7,8]. The swelling capacity of the ASR is closely related to its chemical compositions [9,10]. ASR products generally have a chemical formula of $SiO_2{\cdot}(Na_2O)_n{\cdot}(K_2O)_k{\cdot}(CaO)_c{\cdot}(H_2O)_x$ [11]. The property of the ASR gel is determined by not only the presence of certain elements but also the atomic ratios such as Na/Si, K/Si and Ca/Si [9]. Studies on the role of each element, especially alkali cations, in the ASR gel can help to enhance the understanding of the degradation mechanism of ASR and potentially offer new solutions to mitigate the ASR effect on concrete [10,12].

Different proportions of calcium (Ca^{2+}), sodium (Na^+) and potassium (K^+) in the ASR products can determine their corresponding free swelling capacity [8,9], rheology [11,12], viscosity [13], and morphology [14–19]. Calcium (Ca^{2+}) is noted to be essential for the formation of the precursor of ASR products, C-S-H gel, and one part of the final crystalline ASR products [8,10,13,20]. However, calcium-free ASR products, though amorphous, are also reported to exist in the low-Ca fly ash mortar samples [21]. According to the expansion theories, the internal pressure in samples originated from either the hydrophilicity or crystallization of the ASR gel [9,10]. ASR gels with low or zero Ca are seen as fluids while its solid counterpart in the crystalline Ca-rich form experienced volumetric changes [8,17].

Apart from calcium, alkali cations (Na^+ and K^+) also make a great difference in the formation of ASR products as reflected in different attributes [8–10,13,14,22,23]. K-rich solution dissolves silica slightly slower than Na-rich solution in experimental synthesis and thermodynamic modeling and the corresponding ASR gel is less expansive [16,22]. Many studies mention that K^+ and Na^+ are structurally equivalent in the ASR products but K dominant gel may be somewhat more disordered in molecular structure [9,10,22,23]. Lab synthesis results demonstrate that the crystalline ASR products, Na-shlykovite ($NaCaSi_4O_8(OH)_3{\cdot}2.3H_2O$), are only observed in a sodium dominant environment (Na/Si > 0.25). In contrast, two species of ASR gel are identified in K-containing samples. K-shlykovite ($KCaSi_4O_8(OH)_3{\cdot}2H_2O$) is observed in reaction products when Ca/Si is over 0.3 in the K-containing mixture and a nano-crystalline product labelled as ASR-P1 ($K_{0.52}Ca_{1.16}Si_4O_8(OH)_{2.84}{\cdot}1.5H_2O$) is the other representative ASR gel

* Corresponding author.
E-mail address: gchen@mst.edu (G. Chen).

https://doi.org/10.1016/j.cemconres.2023.107293
Received 22 February 2023; Received in revised form 19 July 2023; Accepted 27 July 2023
Available online 1 August 2023

[10,13]. In the copresence of Na^+ and K^+, the dominant product is ASR-P1 due to the weak stability of shlykovite-like crystalline ASR products [10,24]. The chemical composition of ASR gel may alter its properties. Observations suggest that high alkali/Si increases free swelling capacity but reduces hydrophilicity [13,17]. Synthesized ASR products within a 35 %–75 % relative humidity all exhibit water absorption but this ability for the amorphous ASR-P1 is different from the crystalized Na-/K-shlykovite [9,12]. ASR products with larger cations (e.g., K^+ versus Na^+) is easier to lose H_2O molecules, which is in agreement with the regression model established by Gholizadeh-Vayghan [8,9,22]. However, potassium is reported to yield a comparatively more compact microstructure than that of sodium in synthesized ASR products [25].

Both Na^+ and K^+ can form a high pH environment for the development of ASR, but the expansion of ASR products can be distinct according to their presence [9,14–16,26]. At the nanoscale, the water uptake of Na- and K-dominant ASR gels was investigated using the dynamic vapor sorption (DVS) method and the results illustrated that the synthesized crystalline Na- and K-shlykovite demonstrated no difference in d-spacing in XRD patterns before and after desiccation treatment, which defies the hydrophilic mechanism of the ASR expansion [8,13,24,27]. At the macroscale, Tänzer et al. reported that 1 N inherent K^+ could promote more of length change than Na^+ in GGBFS mortar pastes, while the expansions induced by different cations were close at an alkali's concentration of 0.5 N [14]. On the contrary, Liu and Mukhopadhyay compared the volumetric changes of reactive silica matrix with Na (1 N) and (Na + K) (1 N) and concluded that pure Na^+ yielded more expansion [28]. In addition, the effect of sole alkali on the ASR expansion in concrete was mainly focused on the study of Na in most publications though K is more common in natural existence [8,13]. The coupling effect of both alkali cations, Na and K, on ASR expansion remains inadequately studied in ordinary Portland cement (OPC) based systems.

The quantity of alkalis plays an important role in both the ASR products composition and macroscopic swelling. An innocuous expansion can occur when Na_2O_{eq} is below 0.6 % by mass of binder and the length change remains nearly steady when Na_2O_{eq} is over 4.25 % [29]. The increased amount of alkali is accompanied by a disproportionate expansion [30]. Shehata and Thomas boosted the internal Na^+ from 2.36 % to maximum 5 % in fly ash and the total expansion was positively correlated with the quantity of alkalis in the original cement mix [31]. Wang et al. reported a lower expansion in higher inherent Na-containing OPC samples during the first 70 days of test [16]. Shi et al. tested alkali-activated slag (AAS) with different quantities of Na^+ from 4 % to 8 % and the length change was inversely correlated with the abundance of alkali [32]. It was also found that the onset of ASR expansion is earlier in AAS and the amorphous ASR gel had lower Ca/Si and higher Na/Si ratios than those formed in the corresponding OPC samples [14,32–34]. Tänzer et al.'s research suggested that the ASR expansion induced by Na and K at various alkali concentrations could follow different trends. The elongation of tested samples increased with the amount of Na^+ from 0.5 % to 2 %. In contrast, 2 % K-containing samples were subjected to an average shrinkage of 0.5 mm/m though 1 % K-boosted samples were swelled more than that of Na-boosted. This contrast was possibly attributed to the 'pessimum' effect [14]. Overall, the free swelling capacity due to the quantity of alkalis remains nonconsensual in different cements.

To sum up, both sodium and potassium can exist in ASR products. Currently, there is no consensus on the mechanism of ASR expansions induced by different alkali cations. The objectives of the present study are thus to understand the mechanism of the macroscopical expansion of mortar specimens due to ASR induced by different alkali cations, Na and K, and investigate the cross effect of different cation types in specimens and exposure conditions on the ASR gel composition and volume change. Accelerated ASR tests are conducted with OPC mortar bar specimens at a gradient of boost alkalis in order to quantify their expansion. To understand why mortar specimen expand in exposing solution, the microstructure and elemental composition of ASR products are investigated by means of scanning electron microscopy (SEM) and energy-dispersive X-ray spectroscopy (EDS), respectively in four ASR-prone zones in mortar samples. Moreover, Raman microscopy is also performed to confirm the presence of ASR gels.

2. Materials and method

2.1. Materials

In this study, Type I Ordinary Portland cement (OPC) was used as the binder material with its chemical compositions given in Table 1. The alkali content of the cement is represented by 0.43 % Na_2O and 0.39 % K_2O by weight. The equivalent sodium oxide, Na_2O_{eq}, is calculated by % $Na_2O + 0.658 \times \%K_2O$. Likewise, the equivalent potassium oxide, K_2O_{eq} is determined as $\%K_2O + 1/0.658 \times \%K_2O$. SIMAX® clear glass (containing 80.4 % silica, Table 2) was used as a reactive aggregate. The glass was crushed into small pieces by a grinding machine at a speed of 700 rpm in 30 s and then sieved to the gradation as specified in Fig. 1. Adopted in this study was a gradient of inherent alkali concentrations: con (control, original alkalis), 1.25 %, 2.5 % and 5.0 % in a Na (or K) group, which are designated as Na-con, Na1.25, Na2.5, and Na5.0, respectively. Correspondingly, two reference mixes with 1.25 % alkali and sand aggregates, SNa1.25 and SK1.25, were also included, where the prefix letter S denotes sand aggregates, and the suffix number indicates the percentage of inherent alkali by weight. To reduce their size effect, the sand aggregates were sieved to the same gradation as the glass aggregate [8,34,35]. The inherent alkalis content was boosted by adding extra NaOH/KOH flakes (analytical grade) into the deionized water for mortar mixing.

2.2. Accelerated mortar bar test (AMBT)

To compare the severity of ASR swelling due to various alkali types and quantities, two batches of mortar bar specimens were prepared using an aggregate/binder ratio of 2.25 and a water/cement ratio of 0.47 as specified in ASTM 1260 [36]. For each mix, three bar specimens (25 mm × 25 mm × 285 mm) were cast. After curing in a climate chamber ($T = 23$ °C, RH > 95 %) for 24 h, the mortar specimens were demolded and then subjected to an accelerated mortar bar test (AMBT).

1 N NaOH exposing solution was prepared 24 h before the Na batch of mortar bars was cast to allow time for cooling. Similarly, 1 N KOH exposing solution was prepared for the K batch of mortar bars. Designations of various test samples with a combination of mortar bar specimens with inherent (internal) alkalis and exposing solution with external alkalis are summarized in Table 3. The test matrix in Table 3 includes a K boosted (1.25 %) mix in the Na exposing solution, designated as K1.25-Na, in order to investigate the cation effect of external alkali in the exposing solution. Correspondingly, Na1.25-K represents a Na boosted (1.25 %) mix in the K exposing solution.

All bar specimens were submerged in 80 °C water for one day and then moved into the prepared exposing solution in a sealed container at a temperature of 80 °C for water bath treatment. The length of each specimen was measured at day 0, 1, 3, 5, 7, 14, 21 and 28 with a length comparator (precision: 2 μm). The average measurement of three replicas in a group was reported as the expansion of the group. At the completion of the expansion tests, either small samples or powders are taken from the bar specimens for various material characterization tests.

Table 1
Percentage of oxides in Type I OPC (wt%).

CaO	SiO_2	Al_2O_3	Fe_2O_3	MgO	SO_3	Na_2O	K_2O
64.2	19.8	4.51	3.23	2.76	3.4	0.43	0.39

Table 2
Chemical composition of sand aggregate and glass aggregate (wt%).

	SiO_2	B_2O_3	Al_2O_3	CaO	$K_2O + Na_2O$	Mg_2O	Fe_2O_3
Sand aggregate	76.2	/	11.4	4.0	4.9	1.1	1.51
Glass aggregate	80.4	13.0	2.4	/	4.2	/	/

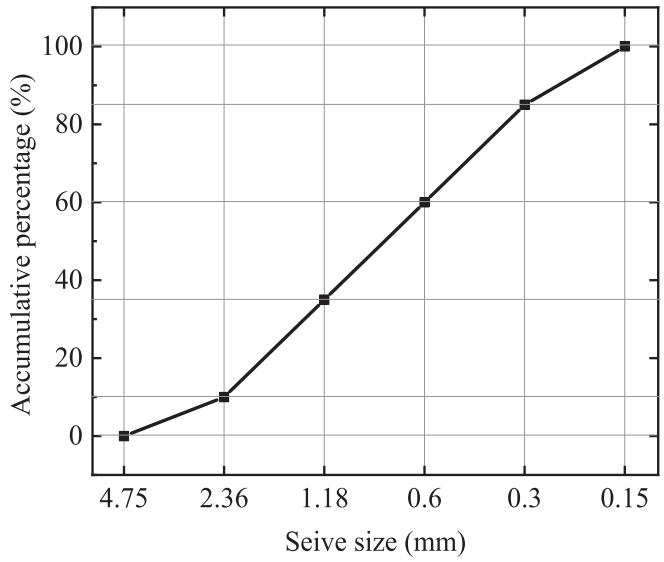

Fig. 1. Gradation of sand and glass aggregates according to ASTM C1260 [36].

2.3. Material characterization tests

2.3.1. Scanning electron microscopy (SEM)/energy dispersive X-ray spectroscopy (EDS)

SEM was performed on polished mortar samples using a Helios Hydra CX with an accelerating voltage of 15 kV and a beam current of 0.8 nA under high vacuum pressure (<5.0E-4 Pa). The working distance between the lens and a sample was set to 4 mm. To determine the atomic composition of the point of interest (POI), EDS was performed with a Thermo Noran Ultra Dry 60 mm^2 detector by point selection in the Pathfinder X-Ray Microanalysis Software. EDS analysis was performed in an automatic precise model and the acquisition time was based on the number of total counts (250,000 counts). The pixel size at the POI was 0.14 μm. Microscopy specimens extracted from ASR specimens after the 28-day AMBT were soaked in 94 % ethanol for 72 h followed by drying in an oven at 50 °C for 72 h. All samples were polished with progressively finer silicon carbide papers (#180, #320, #600, #800, #1200, #2000) to achieve microscopically surface smoothness. Before any SEM/EDS analysis, samples were coated with a thin film of gold/palladium (Au/Pd) by sputtering for 45 s to prevent charging.

2.3.2. Raman spectroscopy

Raman spectra were collected using a Horiba Jobin Yvon LabRAM Arami micron Raman spectrometer (Horiba-Jobin Yvon, Inc., Edison, NJ) with a He-Ne laser (632.8 nm). The laser power, as the excitation source, at the mortar samples was 17 mW. The spots on the samples were pinpointed with a magnification of 50×. Before data collection, the spectrometer was calibrated using the 520.5 cm^{-1} line of a silicon wafer. For each spectrum, 10 runs were performed in 270 s. The spectral range used in this study is 200 cm^{-1} - 1200 cm^{-1} with a spectral resolution of 1 cm^{-1}. The obtained spectra were smoothed with a running of 7 to reduce the noise. In addition, the spectra were background corrected and normalized for comparison between different spots and samples. Preprocessing of the Raman spectra was conducted in Labspec software (Horiba ABX S.A, Kyoto, Japan).

In the Raman spectra, Raman shifts of the different silicate connections are generally located between 400 cm^{-1} - 700 cm^{-1} and 950 cm^{-1} - 1150 cm^{-1}. The shifts can characterize the different Q^n presence in the solids to indicate the complexity of the Si-O connectivity. Q^n denotes the connectivity of a silicate tetrahedron with n bridging oxygens (Si–O–Si), where n ranges from 0 to 4 as depicted in Fig. 2.

3. Results and discussion

3.1. ASR expansion of mortar bars

Fig. 3 summarizes the expansion of mortar bars in exposing solutions after a 28-day exposure to 80 °C water bath. It can be seen that the expansion induced by ASR increases with age, and 90 % of the total length change occurs within the first 7 days. By comparing the accumulative swelling at the end of the AMBT, the length change of Na-boosted mortar bars is found 3 to 4 times as much as that of the corresponding mix in K batch. Boosting Na^+ is prone to enhance the free swelling of the mortar bars, which can also be proven by the length change difference between Na1.25-K and K1.25 in K batch. The more deleterious expansion of the Na batch is attributed to the silica dissolution ability and free swelling capability of the Na-rich ASR products [14,22]. Therefore, extra silica gel is available to be charged by the abundance of the alkalis to form expansive products. This hypothesis is verified by the lower alkali/Si in amorphous gel of Na batch samples as demonstrated in Fig. 6. It can be observed from Fig. 3 that an increased amount of alkali cations boosts the expansion of the test specimen. This trend was also noted in an ASR simulation test with an attempt to determine the *pessimum* effect of alkalis on the ASR [31], although the critical alkalis of 4.25 % in sodium is not confirmed in the present test. In

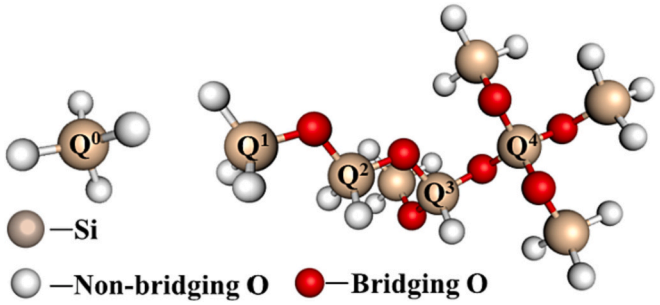

Fig. 2. Schematic demonstration of Q^n.

Table 3
Mortar bar specimens with inherent (internal) alkalis, exposing solution with external alkalis, and sample designation.

Solution	Sand aggregates		Glass aggregates							
	Na (%)	K (%)	Na-boosted (%)				K-boosted (%)			
	1.25	1.25	con	1.25	2.5	5.0	con	1.25	2.5	5.0
1 N NaOH	SNa1.25	–	Na-con	Na1.25	Na2.5	Na5.0	–	K1.25-Na	–	–
1 N KOH	–	SK1.25	–	Na1.25-K	–	–	K-con	K1.25	K2.5	K5.0

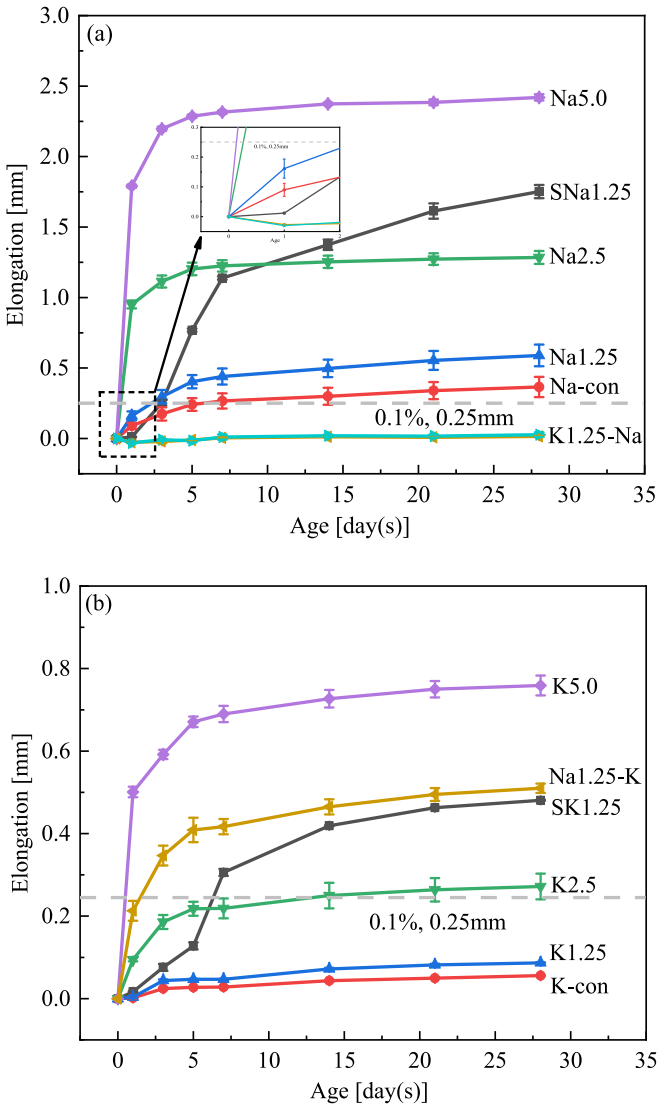

Fig. 3. ASR expansion of mortar bars over time: (a) Na batch, and (b) K batch.

view of the expansion development, the increasing alkalis in the mortar mix accelerates the ASR progress in both batches. The one-day submerge in the exposing solution accomplishes >60 % of the total length change for the mixes with an alkali above 2.5 % and <30 % for the Na1.25, K1.25, and control (con) groups. The acceleration effect is more apparent for the Na batch as Na2.5 and Na5.0 yield a plateau after the first week of the test probably due to the scarcity of the alkalis. At that time, Na-con and Na1.25 were still expanding at a reduced rate.

Effect of the type of alkali cations in the exposing solution on ASR expansion is examined. In Fig. 3(a), Na1.25 in the 1 N NaOH exposing solution experiences a deleterious length change (>0.1 %) while K1.25-Na literally remains at the original length and even experiences a shrinkage after the first-day acclimation in the 80 °C NaOH solution, as indicated in the insert of Fig. 3(a). The shrinkage indicates that the boosting K^+ in K1.25-Na may not be involved in expansion unlike the role of Na^+ for the rest of groups in the Na batch. However, K1.25 in the 1 N KOH exposing solution shows a length increase though innocuous (<0.1 %) as indicated in Fig. 3(b). More importantly, Na1.25-K in the 80 °C KOH solution nearly mimics the length development of the Na1.25 in the 1 N NaOH exposing solution. This contrast indicates that the 1 N KOH solution is innocuous to the length increase of the Na1.25-K. Note that the zero-length change is not reported in Fig. 3(b) because K1.25 and Na1.25-K in the 1 N KOH solution both undergo obvious expansion.

Na^+ in the exposing solution can potentially inhibit the expansion of inherently K-boosted samples. To confirm this new finding, K1.25-Na was repeated. It can be seen from Fig. 3(a) that the two curves nearly overlapped with each other. Both tests coincidentally show the same shrinkage effect after one day of acclimation in the 80 °C NaOH solution. To the best of the author's knowledge, zero expansion observed in the alkali boosted OPC binder is reported for the first time.

3.2. Microstructure and atomic composition

3.2.1. SEM imaging

To investigate the expansion difference between Na- and K-boosted mortar samples, SEM images were analyzed to characterize the microcracks that resulted in the ASR gel expansion and the morphology of the ASR products. Fig. 4 presents the typical microstructures of all mortar mixes obtained from the polished surfaces of their representative bar specimens. It can be seen from Fig. 4 that the dominant cracks are distributed in the aggregates and filled with the amorphous gels. Between the gel and the aggregate are gaps due to the loss of water in the process of desiccation. High alkaline exposure melts the exterior surface of reactive silica aggregates, thus creating a distinct band called interfacial transition zone (ITZ) between an aggregate and its surrounding matrix [8]. No clear morphological difference can be observed between the paste matrix and aggregate vicinity in the present study. Instead, pieces of the obviously molten aggregates are demonstrated as shown in Fig. 4(a-2) and (a-5). Fig. 4(a-2), (a-3), (a-6), (b-1), (b-3), and (b-5) displays void crevices in the mortar matrix in addition to the microcracks on aggregates. Such crevices are much narrower than the aggregate microcracks and thus may be induced by the swelling pressure of the aggregate to the matrix during the ASR [37].

As shown in Fig. 4, the higher the concentration of alkalis, the wider the microcracks in both Na and K batch samples. However, the aggregate crack size in Na batch samples is qualitatively comparable to that in the corresponding K batch samples. To quantify and compare the widths of various aggregate cracks, a total 128 SEM images with crack features were collected to evaluate the degree of macroscopical expansion. Table 4 summarizes the average and standard deviation of crack widths based on the number of measurements. 'Cracks' observed in the mortar samples with sand aggregates, SNa1.25 and SK1.25, look like either the mechanical crevices in Fig. 4(a-1) or the premature silica gel band in Fig. 4(b-1). They are quite different from those observed from other samples and thus excluded from statistical analysis. Independent of the type of alkali cations, the average crack width (thus the ASR severity) increases with the quantity of the alkali. In the test range, the increasing trend is approximately linear up to 5.0 % for K batch samples; but it begins to slow down at 2.5 % for Na batch samples when the crack approaches the maximum width and the ASR gel thus exudates from the aggregates crack to the nearby matrix as indicated in Fig. 5(a-1) due to the excessive pressure. As indicated by the expansion result in Fig. 3, K1.25-Na experiences a negligible length change over the 28-day AMBT. In the SEM analysis, only four cracks are observed in the domain of the K1.25-Na sample. This is another evidence that the external Na^+ may have inhibited the ASR in K-boosted mortar samples.

ASR gels are present in the aggregate cracks, the ITZ, and the mortar matrix in different morphologies due to the availability of Ca^{2+} [8]. As the SEM images in Fig. 4 show, the dominant gel in the aggregate is amorphous. But crystalline ASR products are occasionally observed in the ITZ and the matrix. The amorphous gel in aggregate veins is possibly N-gel and/or K-gel depending on boosting alkalis. The ASR gels in the aggregate veins can be exuded into the matrix as seen in Fig. 5(a-1) through a Na5.0 mortar sample. This is illustrated in Fig. 5(a-2) as the atomic ratios Na/Si and Ca/Si in the aggregate vein are slightly higher than and much lower than those in nearby buffering zones (BZ). The previously documented plate-like or pseudo-rosette crystalline Na-containing ASR products [24] are identified in the BZ of the aggregate crack opening as shown in Fig. 5(b-1). The products present in the BZ are

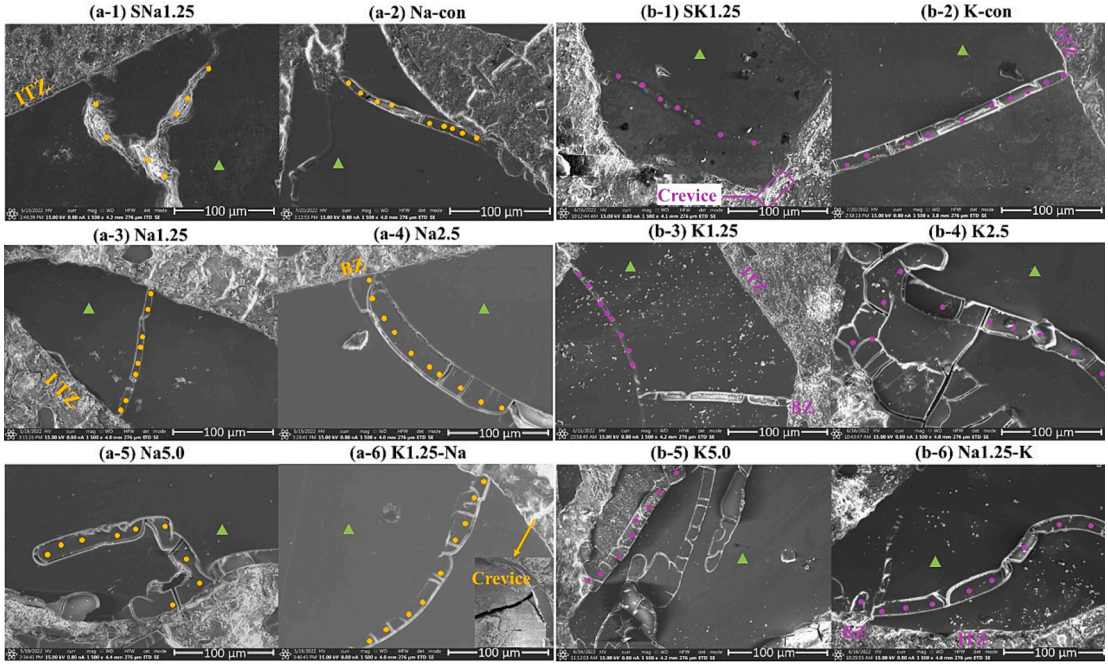

Fig. 4. SEM images to show aggregate microcracks due to ASR in: (a) Na batch, and (b) K batch. Dots along aggregate cracks indicate the POI in EDS and triangles represent aggregates.

Table 4
Statistical results of the crack widths extracted from the SEM images of mortar samples (unit: μm).

Sample	Mean (standard deviation)	No. of cracks	Sample	Mean (standard deviation)	No. of cracks
SNa1.25	/	/	SK1.25	/	/
Na-con	9.87 (3.70)	20	K-con	10.37 (4.15)	16
Na1.25	13.54 (4.45)	19	K1.25	15.93 (7.53)	19
Na2.5	22.37 (5.73)	23	K2.5	19.17 (9.25)	20
Na5.0	24.59 (6.24)	25	K5.0	23.07 (8.62)	22
K1.25-Na	12.32 (5.49)	4	Na1.25-K	16.75 (6.98)	24

Na-shlykovite as confirmed by EDS results in Fig. 5(b-2), although the crystals are smaller than those as described in [24,26] probably due to the short test duration of the present study. In addition, the less isometric needle-like K-containing crystalline ASR products are not observed in K5.0 because of the less expansive K-gel, and the aggregate crack opening remains potentially intact. However, crystalline K-shlykovite is detected in ITZ of K5.0 as shown in Fig. 5(c-1), which can also be assigned as the nanocrystalline ASR-P1 due to the presence of Na by the EDS spectrum (Fig. 5(c-2)).

3.2.2. EDS analysis

According to the current expansion mechanisms, the free swelling capacity of ASR products can be different between morphologies [10]. ASR gel morphology is closely related to its elemental composition, which thus potentially affects the micro-expansion [5–8]. In mortar specimens, the availability of Ca can be restricted due to its limited access to aggregate veins and various morphologies can thus be observed in different spots. As such, statistical analysis of EDS results was performed. The average (and standard deviation) atomic ratios between the essential elements of ASR gels, such as Ca/Si, Na(K)/Si, and (Na + K)/Si, in the veins of aggregates are presented in Fig. 6 for both Na-batch and K-batch samples. The atomic ratios of ASR gels in the crack, BZ, and ITZ are summarized in Table 5 for Na-batch samples and Table 6 for K-batch samples, respectively. For crack statistics, the POIs for EDS analysis in crack are presented in Fig. 4. For BZ and ITZ areas, the number of POIs varies between samples.

3.2.2.1. ASR composition along aggregate cracks. Fig. 6 shows the averaged atomic ratios of the POIs along the aggregate microcrack for each mortar sample. Considering the ASR distribution along cracks from the aggregate-matrix interface to deep aggregate, the small variances of each atomic ratio in both Na and K batch indicate the atomic compositions of those amorphous gel are basically close, which is different from a previous demonstration that the atomic ratio of aggregate gels showed large fluctuations [38]. However, the compositions of the ASR products observed in SNa1.25 and SK1.25 samples seem quite different. This wide difference in ASR products composition is attributed to the uneven distribution of elements in sand aggregate.

With an increasing boosting Na content, Na/Si and (Na + K) gradually decrease and Ca/Si follows a reverse trend. Ca/Si remains at zero in Na-con and Na1.25, and gradually increases to 0.067 in Na5.0. The decrease of alkali/Si with the increasing boosting Na results from two factors: the more dissolved silica gel and the presence of Ca. The more alkali content preserves a high pH environment and thus facilitates the breakage of Si-O in Si tetrahedral, which accelerates the precipitation of Si-O- in the aggregate veins for samples with higher boosting alkalis. In addition, inclusion of divalent Ca (only divalent particles) in ASR gel compensates for two $Si\text{-}O^-$ sites and thus two monovalent cations (Na or K, only monovalent particles) are replaced. In combination with the elemental composition and morphology, it is estimated that Na-gel and dissolved silica are major products in the aggregate cracks for Na-con and Na1.25. For the Ca-containing gels in aggregate cracks in Na2.5 and Na5.0, ASR-P1 ($K_{0.52}Ca_{1.16}Si_4O_8(OH)_{2.84}{\cdot}1.5H_2O$) should coexist with Na-gel and dissolved silica based on the morphological observation. Na-shlykovite might also present but in trivial existence because of Ca. No Ca in the ASR gel seems present along the aggregate cracks due to the inhibition effect of the semi-permeable net (C-S-H) formed in the aggregate vicinity [15,30]. The silicate net allows the passage of Na^+ (227 pm) and K^+ (270 pm) because of their smaller size compared to Ca^{2+} (570 pm). Therefore, Ca^{2+} is prevented from the engagement of the chemical reaction in aggregate veins, which explains the presence of Ca-free amorphous ASR gel. For samples with a higher amount (≥2.5 %) of

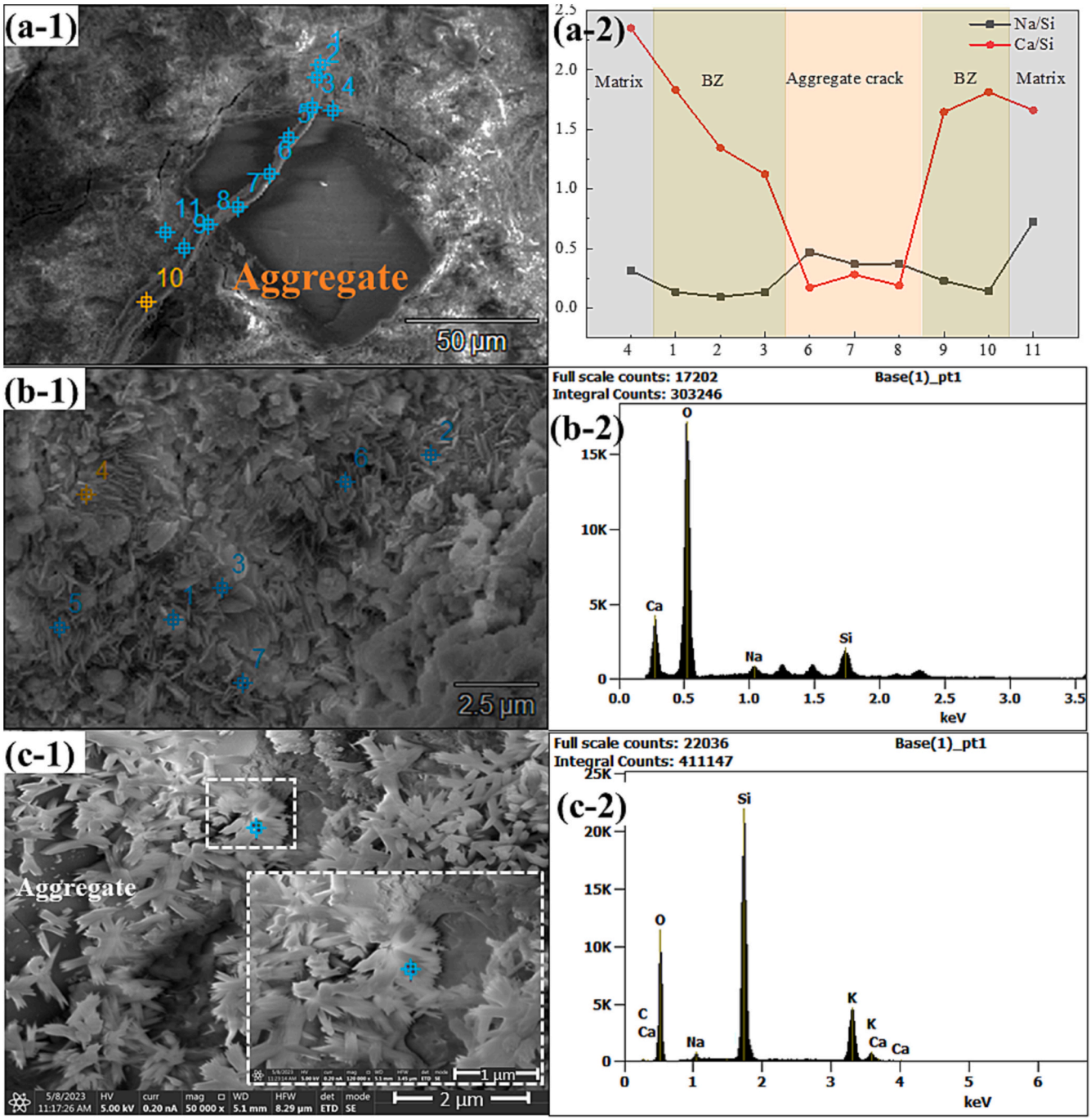

Fig. 5. ASR gel exudation from the aggregate veins to the matrix in Na5.0 sample: (a-1) exudation track and (a-2) atomic ratio along the gel track; (b-1) crystalline ASR products in BZ of Na5.0 and (b-2) EDS spectrum of the crystalline products; (c-1) crystalline ASR products in ITZ of K5.0 and (c-2) EDS spectrum of the crystalline products.

boosting Na, the accumulated internal pressure damages the silicate film and Ca^{2+} accesses to the inner part of the aggregate though the amount is still very limited.

In the K-boosted batch samples, (Na + K)/Si and K/Si remain approximately 0.36 and 0.33 independent of the boosted K, respectively. The alkali/Si is much higher than that in Na batch samples. The high alkali/Si here can be attributed to the less dissolved silica in the aggregate crack because KOH is less aggressive in silica dissolution [22,23]. More interestingly, Ca^{2+} is absent in all the K-boosted samples as the Ca/Si ratio stays at zero. It is believed that the C-S-H film remains intact to resist the internal swelling pressure and prevents the Ca ingress. Likewise, it is reasonable to assume that the amorphous gel in aggregates is K-gel and molten silica in all K dominant cases. In combination with the crack width, Na5.0 yields an averaged larger crack width than that of K5.0, and ASR gel exudation only happens in Na5.0. This observation can be related to the findings that the K-gel contains less water and thus probably less expansive as larger alkali cations in the interlayer of the silicate chain cannot retain H_2O effectively [10]. Therefore, the weaker hydrophilicity of K-containing ASR gel cannot produce tantamount pressure like Na-containing samples to impair the C-S-H film.

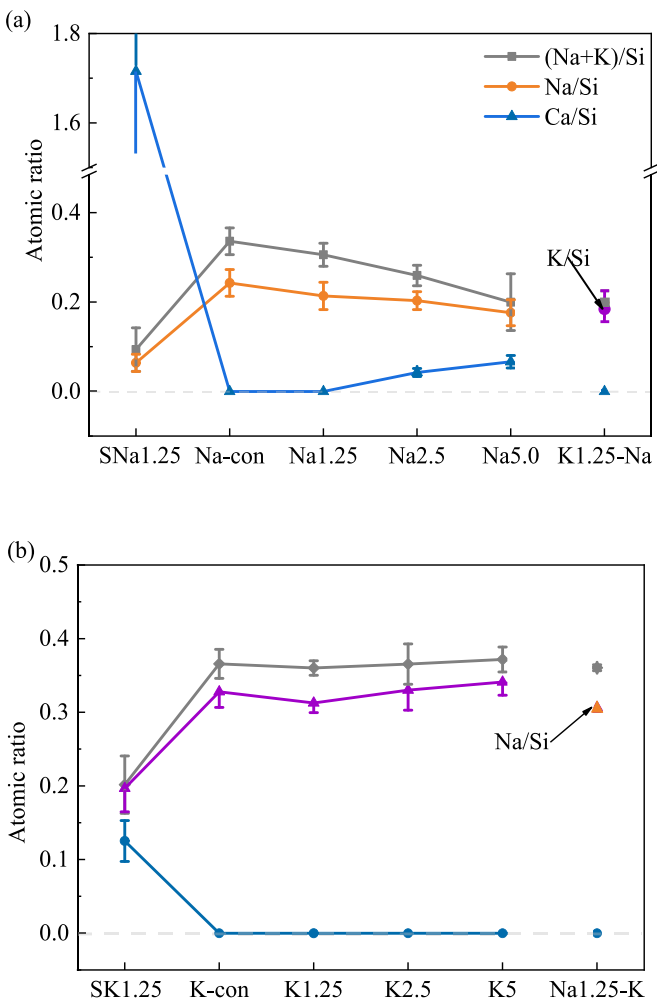

Fig. 6. Atomic ratios of ASR gels in aggregate veins of: (a) Na-batch, and (b) K-batch samples.

Gels in aggregate vein of K1.25-Na possess similar alkali/Si as opposed to Na1.25. Ca^{2+} is still absent in the crack gel. The results indicate that the amount of dissolved silica in crack is more likely regulated by the exposing solution otherwise K/Si should be close to K batch samples, which is also applicable for Na/Si in Na1.25-K in KOH exposing solution. In addition, it is found that the major alkali presence in aggregate vein is in line with the boosting alkali type for both K1.25-Na and Na1.25-K. The observation implies that the inherently boosting alkalis is more effective in the gel formation in aggregate cracks than the Na(K) in the exposing solution.

3.2.2.2. Gel compositions in potential ASR zones. The most reported spots that contain ASR gels are the aggregates cracks and ITZ due to the availability of silica gels [13,14,20]. They observed some ASR products exudations from the aggregates to their nearby mortar matrix where Ca^{2+} is highly attainable. Ca^{2+} plays a role in both gelation and crystallization in ASR and therefore the buffering zone (BZ) of the ASR aggregate crack is also selected to be the region of interest [20]. As shown in Tables 5 and 6, alkali/Si drops, and Ca/Si increases in both Na- and K-batch samples from the crack through ITZ to the BZ. Ca^{2+}, a bivalent element, competes with monovalent alkalis and takes more places on the Q^n species $Si\text{-}O^-$ sites to compensate negative charges [39–41]. This finding consolidates the 'alkali cycling' effect that alkalis are liberated due to the presence of Ca^{2+} but defies the notion that alkalis are not released but still absorbed by the ASR gel via the van der Waals force in a molecular dynamic simulation [6,7,41]. Alkalis ratio (Na(K)/Si, (Na + K)/Si) of the ITZ for Na- or K-boosted samples are close to that of the aggregate gels and ranges from 0.20 to 0.40. Such alkali/Si ratios were also reported in the ASR products in the previous studies [9,14,19,30]. Therefore, ASR products might also be present in the ITZ.

In BZ, Ca/Si exceeds 2.0 for Na-con and Na1.25, but 1.36 and 1.69 for Na2.5 and Na5.0, respectively. In contrast, Ca/Si all reaches over 2.0 in the K-boosted samples. High Ca/Si demonstrates that the products in the BZ are mainly C-S-H since Ca-containing ASR gels possess a much lower Ca/Si [10,41]. In this regard, ASR products should account for the low Ca/Si for Na2.5 and Na5.0 due to the ASR gel exudation. Though an obvious ASR gel exudation is not observed in Na2.5, a clear ASR gel track in Na5.0 is captured by SEM. The corresponding crystalline ASR products and elemental compositions are demonstrated in Fig. 5. The

Table 5
Atomic ratios of the potential ASR gels in different zones of Na batch mortar samples. The italic number denotes a K/Si ratio in the corresponding mix. Results are presented in the format of mean (standard deviation).

	(Na + K)/Si			Na/Si			Ca/Si		
	Crack	ITZ	BZ	Crack	ITZ	BZ	Crack	ITZ	BZ
SNa1.25	0.09 (0.05)	0.35 (0.16)	0.04 (0.02)	0.06 (0.02)	0.14 (0.03)	0.14 (0.10)	1.72 (0.78)	2.70 (0.21)	5.67 (1.95)
Na-con	0.34 (0.03)	0.25 (0.07)	0.16 (0.06)	0.24 (0.03)	0.23 (0.07)	0.12 (0.05)	0 (0)	1.49 (0.32)	2.85 (1.21)
Na1.25	0.31 (0.03)	0.17 (0.05)	0.14 (0.05)	0.21 (0.03)	0.14 (0.09)	0.11 (0.06)	0 (0)	1.21 (0.06)	2.9 (1.45)
Na2.5	0.26 (0.02)	0.13 (0.04)	0.11 (0.03)	0.20 (0.02)	0.11 (0.30)	0.11 (0.03)	0.04 (0.01)	1.02 (0.37)	1.36 (0.51)
Na5.0	0.20 (0.06)	0.22 (0.08)	0.18 (0.09)	0.18 (0.03)	0.21 (0.08)	0.17 (0.09)	0.07 (0.01)	1.96 (0.33)	1.69 (0.48)
K1.25-Na	0.20 (0.03)	0.16 (0.06)	0.21 (0.08)	*0.18 (0.04)*	*0.14 (0.05)*	*0.22 (0.08)*	0 (0)	0.84 (0.47)	2.96 (0.93)

Table 6
Atomic ratios of the potential ASR gels in different zones of K batch mortar samples. The italic number denotes a Na/Si ratio in the corresponding mix. Results are presented in the format of mean (standard deviation).

	(Na + K)/Si			K/Si			Ca/Si		
	Crack	ITZ	BZ	Crack	ITZ	BZ	Crack	ITZ	BZ
SK1.25	0.20 (0.04)	0.14 (0.04)	0.25 (0.03)	0.20 (0.03)	0.13 (0.04)	0.17 (0.06)	0.13 (0.03)	0.13 (0.01)	4.57 (1.29)
K-con	0.42 (0.02)	0.18 (0.06)	0.21 (0.07)	0.39 (0.02)	0.15 (0.05)	0.18 (0.08)	0 (0)	1.11 (0.71)	2.79 (1.12)
K1.25	0.36 (0.01)	0.29 (0.01)	0.19 (0.06)	0.31 (0.01)	0.21 (0.02)	0.18 (0.07)	0 (0)	1.77 (0.63)	3.00 (1.34)
K2.5	0.37 (0.03)	0.27 (0.02)	0.17 (0.07)	0.33 (0.03)	0.22 (0.02)	0.16 (0.06)	0 (0)	1.85 (0.44)	2.58 (1.02)
K5.0	0.37 (0.02)	0.23 (0.11)	0.16 (0.04)	0.34 (0.02)	0.20 (0.10)	0.13 (0.05)	0 (0)	1.11 (0.88)	2.31 (0.9)
Na1.25-K	0.36 (0)	0.19 (0.06)	0.2 (0.07)	*0.31 (0.01)*	*0.13 (0.65)*	*0.18 (0.06)*	0 (0)	1.57 (0.69)	2.84 (0.9)

atomic ratios along the ASR gel exudation trace in Fig. 5(a-2) match well with the results obtained from different zones in Table 5. In addition, some crystalline ASR products are also detected in ITZ of K5.0 as shown in Fig. 5(c). Therefore, crystalline ASR products should also avail mortar expansion as implied by the previous studies which illustrate the main ASR products are in crystalline form [42].

3.3. Raman spectroscopy

Raman spectra of the crystalline (Na-shlykovite and K-shlykovite) and nanocrystalline (ASR-P1) ASR products have been revealed in lab syntheses [10]. In addition, such ASR products were also characterized by Raman spectroscopy in in-service concrete and mortar samples after accelerated ASR test [10,27,42]. Raman spectra of some representative ASR products are presented in Fig. 7. ASR products in different morphologies display significant differences in Raman spectra. Previous studies indicate that ASR products, especially the crystalline form, are mainly present in the vein of silicate aggregates, though the air voids in ITZ also observed its presence [42,43]. Amorphous ASR products are present near (usually within 30 μm) the vein opening as well as in ITZ and the trace of aggregate gel exudation [43]. As a result, four zones, deep vein (vein-deep, >200 μm from aggregate-matrix interface), vein opening (vein-open, <20 μm from aggregate-matrix interface), ITZ and BZ, are examined by Raman microscopy in this study to locate the potential occurrence of the ASR gels.

Figs. 8 and 10 show the comparison of Raman spectra between the four zones from different mortar groups in Na and K batch, respectively. Distinguishable Raman spectral features can be located in two distinct ranges, 950 cm^{-1} - 1150 cm^{-1} and 450 cm^{-1} - 750 cm^{-1}. For ASR products, the peaks and envelop in 450 cm^{-1} - 750 cm^{-1} are attributed to the symmetric bending (SB) of the silica-oxygen (Si-O-Si) linkages [10,44,45]. More specifically, 430 cm^{-1} - 465 cm^{-1} is related to internal deformation (Q^4 linkage) of the silicate units [10,43]. 590 cm^{-1} - 650 cm^{-1} is assigned to the Q^3 units of Si-O-Si and Q^2 sites are previously correlated with the peak in 686 cm^{-1} - 688 cm^{-1} [10,27]. High-frequency region, 950 cm^{-1} - 1150 cm^{-1}, are attributed to the symmetric stretching (SS) of Q^n species in silicate tetrahedra connections. Q^2 sites of Si-O-Si (typically in chain structure) are in 950 cm^{-1} - 1030 cm^{-1} and 1060 cm^{-1} - 1120 cm^{-1} is assigned to the Q^3 Si units. However, the symmetric stretching of the C—O polyhedral is also reported to yield a resolved peak in this range around 1088 cm^{-1} [10,44,45].

3.3.1. Raman spectra of Na batch samples

Fig. 8 presents the Raman spectra extracted from mortar samples in the 1 N NaOH exposing solution after 28 days. Raman spectra in the aggregate vein (vein-deep and vein-open) of SNa1.25 resemble because both show multiple unresolved peaks in the low-frequency region and a dominating peak at 1088 cm^{-1} which is observable in other samples. It is noted that Raman spectra in BZ and ITZ are almost identical to denote the similar gels in those zones. However, the peak at 465 cm^{-1} distinguishes from the rest samples.

For samples with glass aggregates, Na-con and Na1.25 both display similar Raman spectra at different zones. In the aggregate vein, vein-deep and vein-open yield a broad peak centered at 462 cm^{-1} with multiple shoulders. The resembling broad peak feature was also reported in the synthetic Na-gel and K-gel (without Ca) [44,46]. In addition, shoulders can be identified in 495 cm^{-1} - 520 cm^{-1} to illustrate the presence of Q^3 Si-O-Si in aggregate vein gels, which can be attributed to the involvement of Na because Na/K is known as silicate network modifier [22,44]. The presence of Na is also confirmed by the EDS results. As a result, the amorphous products in aggregate veins can be attributed to the substantial dissolved amorphous silica gels and Na-gel. Moreover, the Raman spectra along the vein are highly reproductive to demonstrate the uniform composition of the mixture, which is in line with the trivial variance of each detectable element as shown in Table 5. In high frequency, vein gels yield a broad peak ranging from 970 cm^{-1} to 1140 cm^{-1} though it is less significant in Na-con. The peak centered at 1070 cm^{-1} is representing the SS of Q^3 units in Si tetrahedra in synthesized ASR-P1 [10], which agrees with the Q^3 presence in the low-frequency region. In this regard, the gels in BZ and ITZ can also be attributed to dissolved silica due to the similar Raman spectra. It is also noted that Na-con and Na1.25 observed a resolved peak near 1088 cm^{-1}, which is contributed by C—O due to the carbonization in the matrix. For Na2.5 and Na5.0, more resolved peaks are detected in all four zones of interest due to the more engagement of Ca to demonstrate the existence of crystalline products because Ca is essential for the crystallization of ASR products [42].

In Na2.5, a more resolved peak at 600 cm^{-1} is detected in vein-deep compared to vein-open. Moreover, both zones yield the strongest peak at 1090 cm^{-1}. A single sharp 600 cm^{-1} peak (SB, Q^3 sites Si-O) in accompany by the resolved 1088 cm^{-1} (SS, Q^3 sites Si tetrahedra) was reported to characterize the Na-shlykovite (crystalline Na-containing ASR products) in the syntheses, mortar and concrete samples [10,27,42]. The band in 970 cm^{-1} - 1140 cm^{-1} is much broader in this

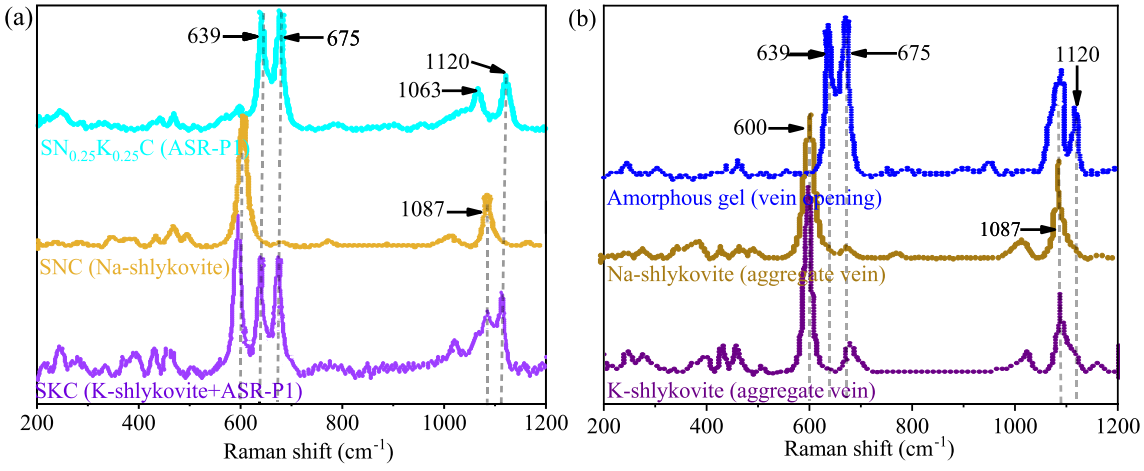

Fig. 7. Raman spectra of (a) synthetic ASR products from [10], and (b) the observed ASR products in aggregate veins of mortar samples in 80 °C NaOH/KOH exposing solution [42].

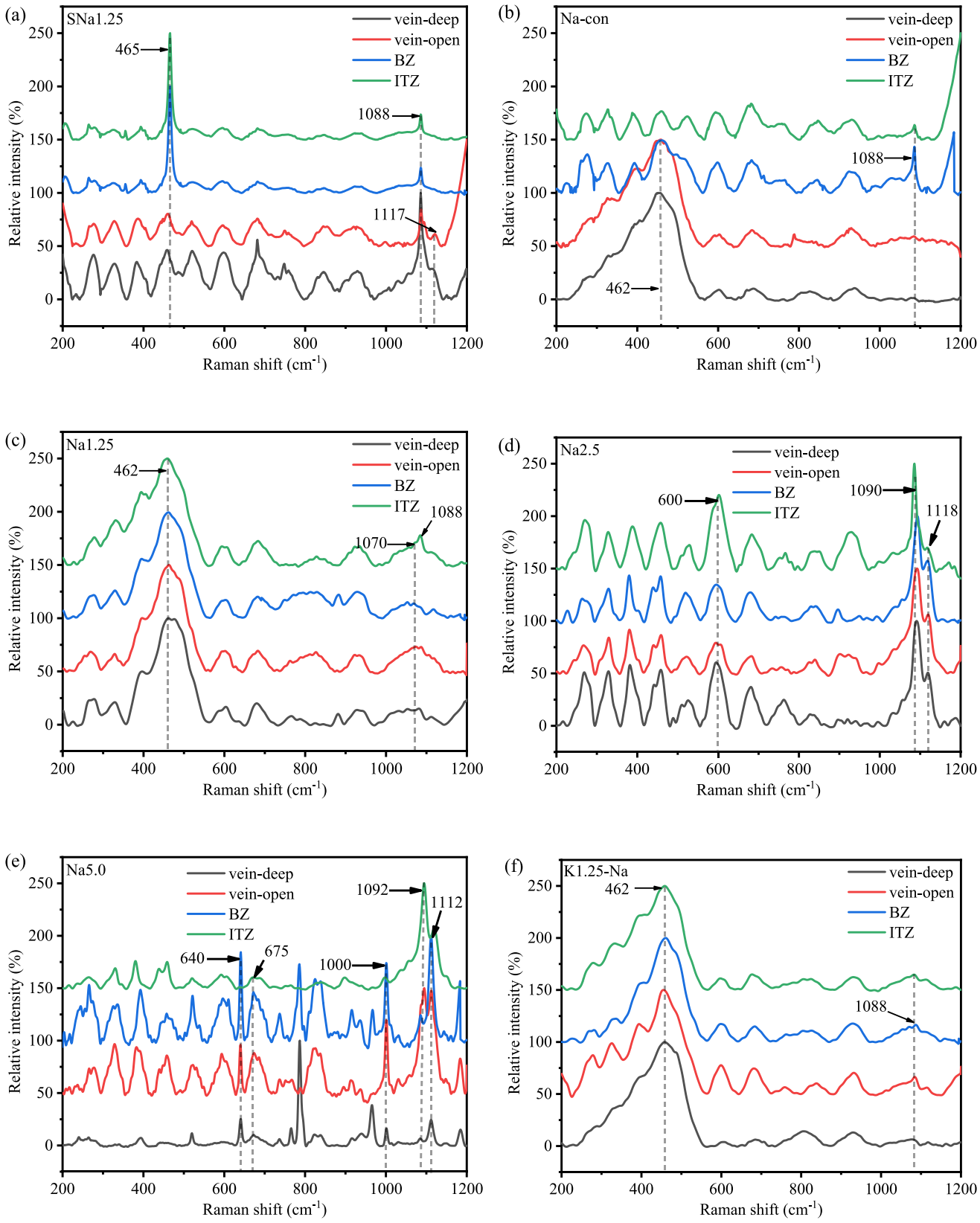

Fig. 8. Raman spectra at different zones of the Na batch samples: (a) SNa1.25, (b) Na-con, (c) Na1.25, (d) Na2.5, (e) Na5.0, and (f) K1.25-Na.

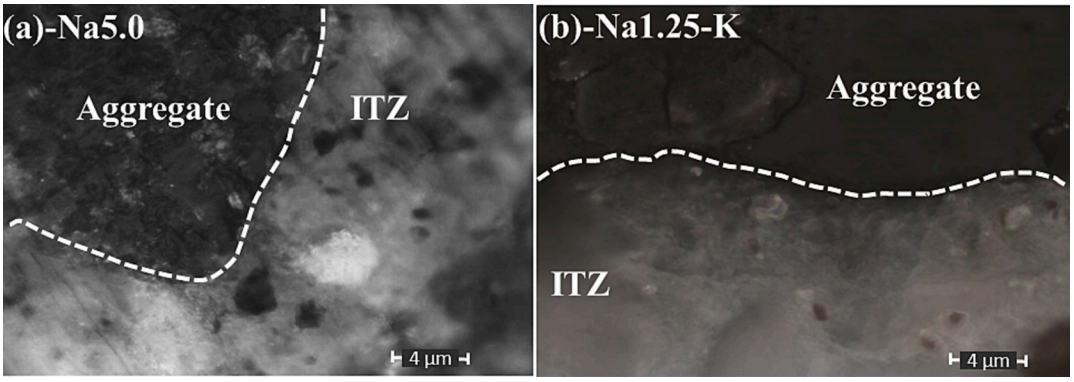

Fig. 9. Crystals in ITZ of sample Na5.0 and Na1.25-K with a microscopic magnification×50.

study, which denotes that the Na-shlykovite and dissolved silica gel should coexist in aggregate vein, BZ and ITZ. EDS results also show the accumulation of Ca in aggregate vein to support the potential crystallization of ASR products though no Na-shlykovite is not observed in SEM, which is probably because of its insignificant existence (Ca/Si = 0.04). As for BZ and ITZ, both zones yield similar Raman spectra as vein gels to demonstrate similar gels' existence. Na5.0 overall observed more resolved peaks in Raman spectra than Na2.5 and a unique peak 640 cm^{-1} over the rest samples at Na batch samples. The placement of resolved peaks at 640 cm^{-1}, 675 cm^{-1}, and 1112 cm^{-1} with a shoulder at 1088 cm^{-1} in vein-deep is almost the same as the amorphous ASR-P1 in aggregate of mortar samples after accelerated ASR test [10,42]. This Raman spectrum also resembles the synthetic ASR-P1. As ASR-P1 was only observed in K-containing environment, the presence of potential ASR-P1 in the aggregate vein in Na boosted samples in NaOH exposing solution can be explained by the K in aggregate as well as the intrusion from the mortar matrix. The dominating peak at 795 cm^{-1} is unattributable, which is also detected in the amorphous ASR gel in [27,43]. Raman spectra in vein-open and BZ resemble and also observe the sharp peaks in vein-deep. In comparison, spectra at BZ are more resolved to illustrate the more crystalline ASR products herein. A resolved peak at 600 cm^{-1} is detected in BZ, which was assigned as the representative peak for Na-shlykovite [42]. Therefore, it is suggested that amorphous ASR-P1 and dissolved silica co-present at vein-open and Na-shlykovite is the dominating ASR products in BZ. The presence of isometric plate-like Na-shlykovite was detected in BZ of Na5.0 as shown in Fig. 5(b-1). In addition, ITZ is filled with dissolved silica and probable amorphous ASR-P1 as indicated by the peak features at 1050 cm^{-1} - 1120 cm^{-1}. Moreover, the microscope×50 also found some transparent crystals in aggregate vein and ITZ in Na5.0 as shown in Fig. 9.

For the K-boost (1.25 %) sample in 1 N NaOH exposing solution, Raman spectra in the aggregate, BZ, and ITZ are almost the same and are highly alike the spectrum that presents the mixture of dissolved silica Na-gel. As both Na-gel and K-gel both yield broad bands in the low-frequency region, it is reasonable to assume that K-gel and dissolved silica dominate all four zones in K1.25-Na in combination with EDS results.

3.3.2. *Raman spectra of K batch samples*

SK1.25 produced some distinct resolved peaks as of SNa1.25 in the low-frequency region (200 cm^{-1} - 600 cm^{-1}). Besides the peak at 450 cm^{-1} in SNa1.25, Raman peaks within 200 cm^{-1} - 350 cm^{-1} are attributed to C—O polyhedral and lattice vibrations, and 400 cm^{-1} - 500 cm^{-1} is assigned to the internal deformation of the Si-O tetrahedra (SB, Q^4 units of O-Si-O) [10]. The products in those four spots of interest are not clear based on the Raman spectra without showing more peak features.

For the mortar samples with different amounts of boosting K, Raman spectra do not show significant differences among vein-deep, vein open and BZ. All spectra are composed of multiple unresolved peaks in the low-frequency region and a broad band in 950 cm^{-1} - 1140 cm^{-1}. The broad band contains a dominating peak near 1088 cm^{-1} with a shoulder at 1117 cm^{-1}. With the given element composition in Table 6 as well as the analysis in Na batch samples, the products in aggregate vein are mainly K-gel and dissolved silica. BZ is occupied by the dissolved silica and some mixtures with Ca, Na, and K. Unlike the Raman spectra in Na batch, no diagnostic peaks, mainly appearing in 600 cm^{-1} - 700 cm^{-1}, for amorphous and crystalline ASR products are detected in K batch. For the spectra in ITZ, a small peak is observed at 635 cm^{-1} in K-con, K2.5 and K5.0, which was assigned to the Q^3 units of Si-O-Si in amorphous ASR products and ASR-P1 [10,42]. Therefore, it can be assumed that amorphous ASR gels should exist in ITZ of these three mortar samples.

For Na1.25-K, Raman spectra show a strong indication of amorphous gels in the aggrege veins according to the spectral profile in vein-deep and vein-open because similar spectra are also observed in the Na batch samples. Likewise, gels in veins should be a mixture of Na-gel and dissolved silica. For BZ and ITZ, a similar peak distribution is displayed between two zones where three peaks in 600 cm^{-1} - 700 cm^{-1}, double peaks presence in 1080 cm^{-1} - 1120 cm^{-1} and the dominating peak at 1000 cm^{-1} are detected. The presence of the resolved peaks indicates that the ASR products in those zones are mainly crystalline and nanocrystalline. A similar triple peak arrangement was reported in the synthesized crystalline K-containing ASR products which should contain both K-shlykovite and ASR-P1 [10]. However, the peak at 600 cm^{-1} in the synthesis samples shifts to 621 cm^{-1} while the other two peaks (640 cm^{-1} and 676 cm^{-1}) display the same peak placement compared to the Raman spectra in BZ and ITZ of Na1.25-K. Moreover, the peak at 676 cm^{-1} is less resolved in this study. In addition, the sharp peak at 1113 cm^{-1} (SS of Q^3 units in Si tetrahedra) and 1000 cm^{-1} (SS of Q^2 units in Si tetrahedra) collaboratively denote the presence of crystalline ASR products in those zones. Moreover, Na1.25-K also observed some crystals as illustrated in Fig. 9 in ITZ.

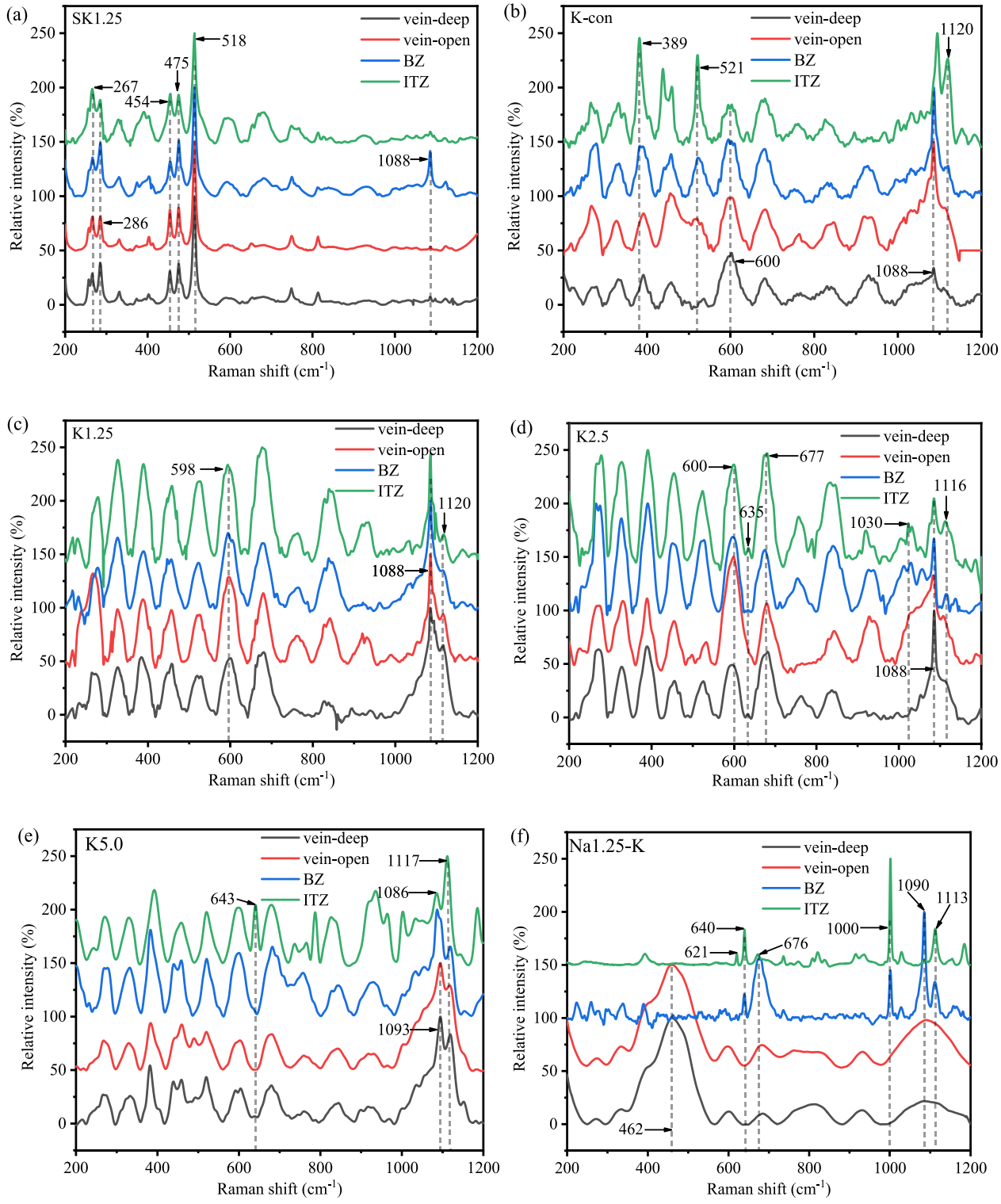

Fig. 10. Raman spectra at different spots of the K batch samples: (a) SK1.25, (b) K-con, (c) K1.25, (d) K2.5, (e) K5.0, and (f) Na1.25-K.

3.4. Further discussion about ASR expansion

The Raman microscopy in accompany with SEM and EDS results show that different morphological ASR products are present in the mortar samples after the accelerated ASR test. Product morphology, specifically crystalline and nanocrystalline, is basically regulated by the attainability of Ca [10,43]. Four zones where ASR products were reportedly present are investigated to locate the potential existence of the previously identified ASR products. Crystalline (Na-shlykovite and K-shlykovite) and nanocrystalline (ASR-P1, which can be amorphous in concrete) were generally reported in the aggregate veins. Both types of ASR products are featured by the involvement of Ca in the chemical composition. More specifically, crystalline ones are present in deep veins while amorphous is usually observed in the vicinity of vein opening [42]. However, the SEM results demonstrate that no crystalline ASR product is visible in the aggregate vein independent of the boosted alkali

quantity and type in this study. Some amorphous ASR-P1 may exist in the aggregate veins but only in Na2.5 and Na5.0 because Raman spectra show a diagnostic peak at 635 cm^{-1}. EDS results also support this conclusion due to the presence of Ca in the aggregate vein. For the rest samples in Na and K batch with glass aggregates, vein gels are composed of Na-gel/K-gel and dissolved silica. The ASR products' existence in aggregate vein in this study is significantly different from the previous publications which demonstrated a clear presence of crystalline and amorphous ASR products. However, the detrimental expansion is still observed in most mortar samples despite the boosted alkali quantity and type. Thus, the expansion source due to ASR products in mortar samples is divided into two parts, aggregate veins, and aggregate vicinities (BZ and ITZ).

3.4.1. Expansion by ASR products in aggregate veins

Almost all ASR studies in concrete and mortar samples reported the cracking of the aggregates. It is reasonable to link the expansion with the micro cracks in aggregates. The fillings in the aggregate vein can directly affect the severity of the cracking. This hypothesis is in agreement with a study that illustrated the swelling mortar/concrete might originate from the expansion of silica aggregate [47]. Comparing the gels in aggregate vein in Na and K batch, similar gel compositions are detected without considering the alkali cations' type. However, the accumulated expansion after 28-day AMBT for Na boosted mortar prisms is 20 %–350 % more than the corresponding mix in the K-boost group. The substantially larger expansion of mortar specimens in NaOH exposure was also observed in [42]. The difference can be compromised by the finding that Na-gel can absorb more water within the gel bulks than K-gel. That more water containment on Na-gel was illustrated in DVS results of the synthetic Na-gel in [10]. When the gels are confined within the aggregate veins by the semi-permeable C-S-H net, Na-gel together with water retainment occupies a large volume and thus yields more pressure in aggregate vein to enlarge the crack width, which agrees with the statistical crack width result in Table 4. A recent study revealed that confined Na-gel developed faster expansive pressure than K-gel and a 13.2 % higher pressure was noted in Na-gel at day 3 [46]. That also explains the sharper expansion curve for Na batch samples at the first week of the test as shown in Fig. 3. In addition, the internal pressure in aggregate veins is also expected to facilitate the length development. The length of aggregate vein varies significantly depending on the dimension of the aggregates. Therefore, its contribution to the length changes of mortar specimens is not quantified yet. Moreover, the more aggressive Na-dominating environment eases the dissolution of reactive silica and might be responsible for the more Na-gel in aggregate vein [22,23].

As for the Ca-containing ASR products in aggregate veins, crystalline ASR products can be present though amorphous ASR-P1 is more likely as the ASR products according to the Raman spectra peak placement. The effect of calcification on ASR expansion can be divided into two parts, the volume change of Ca-containing ASR products due to water sorption and the volume change due to Ca presence from Ca-free gels. A previous study indicated that the crystalline Na-shlykovite did not show any basal spacing change before and after the drying process, which is also applicable to K-shlykovite [10,24]. Therefore, the notion that the water sandwiched in the interlayer accounts for the expansion can be excluded. As such, it is believed that water is absorbed on the surface of the layer structure in Na-shlykovite and K-shlykovite. The current research does not show a clear relation between volume rise and water sorption in crystalline ASR products. If the Ca-containing ASR product is ASR-P1, previous studies indicate that only an insignificant portion of its existence is detected in aggregate veins [27,42,43]. Moreover, the water uptake capability and retainability are not investigated. In addition, Ca-rich ASR products are not expected to possess a water-suction ability [42]. Overall, the volume change by water sorption of the Ca-rich ASR products is not likely to explain the deleterious swelling on mortar samples.

On the other hand, the engagement of Ca in the Na-gel (K-gel) in the synthetic sample was reported to yield more expansion pressure. Reference [48], as shown in Fig. 11(a), demonstrated that the expansion pressure is almost doubled when Ca/Si increases from 0.15 to 0.3 for the gel with a Na/Si of 0.55. In the meantime, the more Ca in this gel mixture yielded a 2.5 % length increase as illustrated in Fig. 11(b) (gel prism, 12.7 mm × 12.7 mm × 127 mm) [9]. In another study, a similar higher swelling pressure was reported to be induced by Ca-containing Na-gels with more Ca [49]. In this regard, it is estimated that calcification of the Na-gel in aggregate vein can also contribute to the swelling of cracks and maybe progressively affect the macro expansion in mortar bars.

3.4.2. Expansion by ASR products out of aggregates

Besides the ASR gel presented in the domain of aggregates, some nanocrystalline ASR-P1 and crystalline ASR products are also detected in BZ and ITZ as indicated by Raman spectra, SEM (Fig. 5) and optical microscope results (Fig. 9). Plate-like Na-shlykovite was observed in the BZ of sample Na5.0 and the less isometric elongated crystallized ASR products were present in the ITZ of K 5.0 and Na1.25-K. The crystalline ASR products in K 5.0 can be a mixture of K-shlykovite and ASR-P1 because both products show elongated needle morphology [10,42]. The alignment of triple peaks in 600–700 cm^{-1} of the corresponding Raman spectra can also support their co-presence. Likewise, Na-shlykovite and ASR-P1 may coexist in the ITZ of Na1.25-K. In addition, it is worth noting that some amorphous gels also exist in ITZ and BZ due to the observation of broad bands in Raman spectra in the high-frequency region, especially for the samples in K batch.

According to the expansion mechanism by ASR products, the water uptake theory is not applicable in this case for Na(K)-gel and other Ca-containing ASR products out of aggregates. In comparison with C-S-H, all types of reported synthetic ASR products contain less water according to DVS results [10]. C-S-H as the main hydration product in ordinary concrete produced a 1.0–1.5 ‰ volume swelling when the relative humidity increased from 70 % to 98 % [50]. More C-S-H can be expected to appear in the mortar matrix in this study because all the test specimens are cultivated in highly alkaline exposing solutions. A thermodynamic modeling illustrates that the formation of C-S-H is prioritized and enhanced over ASR products in high PH environment [20,42]. As for the potential expansion effect by calcification for the Ca-containing ASR products, it has been elaborated in Section 3.4.1. The volume change of ASR gels included by calcification has not been investigated. Instead, some studies focused on investigating the properties, such as rheology and water uptake capacities, of Ca-containing ASR gels to validate the hypothesis that water sorption accounts for the expansion [41,46,49]. However, Shi etc. revealed that water intake cannot be the main reason for ASR expansion for crystalline ASR products [10,42]. In addition, a molecular dynamic simulation demonstrated that the calcification of the shrinks ASR gel volume and increased the solidification of gels [41]. Therefore, it is worth studying the effect of calcification on ASR expansion.

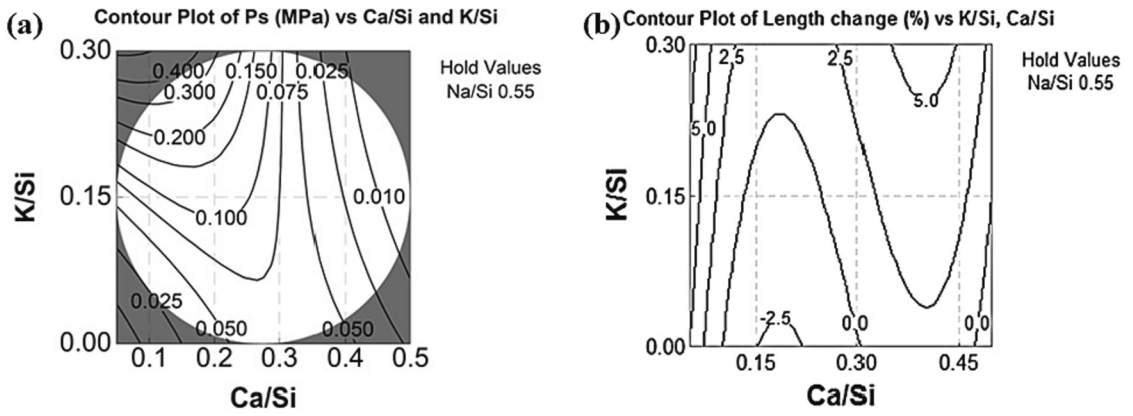

Fig. 11. The contour plots of (a) swelling pressure (P_{rs}) of confined gels [48], and (b) length change (%) of gel prisms (12.7 mm × 12.7 mm × 127 mm) [9], as a function of Ca/Si, Na/Si, and K/Si.

4. Conclusions

This study investigated and quantified the effect of boosting alkali types, Na and K, on the ASR expansion of OPC mortar samples. Expansion results were presented to show the severity of the ASR. Microscopic analysis was conducted with SEM to locate the potential presence of the ASR gel and examine the corresponding morphology. The chemical compositions of ASR products were identified with EDS to understand the expansion mechanism behind different ASR products. The presence of potential ASR products was also evaluated by Raman microscopy. Based on the extensive laboratory tests, the following conclusions can be drawn:

1. The increase of boosted alkalis (Na or K) accelerated the ASR development resulting in the expansion of OPC mortar samples. Na batch samples expanded approximately three times as much as corresponding K batch samples.
2. ASR gels were mostly observed in the veins of aggregate and ITZ with a small percentage appeared in the paste matrix due to gel exudation. Gels in the domain of aggregates were amorphous. The crystalline plate-like ASR products were observed in the matrix due to their contact with Ca^{2+}.
3. ASR gel in aggregate is generally free of calcium and the atomic ratios for samples within batch (Na- and K-) are close. The presence of Ca^{2+} in the aggregate ASR gel reduced Na/Si though the gels remained amorphous. Crystalline ASR products in the matrix of cement paste contained more Ca^{2+} and fewer alkalis (Na and K) than those in the aggregate crack ASR gel.
4. The effect of boosting alkali cations is more effective in the composition of ASR products than in the exposing solution. Na^{+} in exposing solution prevented the development of aggregate cracks in K-boosted samples while an external K^{+} exposure did not show such an inhibitation effect for Na-boosted samples.

Future studies will be directed to investigate the ASR expansion mechanism proposed in this study. In particular, the potential ASR products presented in this paper will be synthesized to test the volume change due to either crystallization or water uptake and compare Na- with K-containing samples. The effect of calcification and hydrophilicity on the swelling ability will be compared and quantified.

CRediT authorship contribution statement

Pengfei Ma: Conceptualization, Methodology, Validation, Formal analysis, Investigation, Writing original draft, Writing -review & editing, Visualization. Ying Zhuo: Methodology, Validation. Zhenhua Shi: Methodology. Jincheng Bai: Methodology, Writing -review & editing. Linyu Chi: Methodology, Writing review & editing. Genda Chen: Conceptualization, Methodology, Investigation, Formal analysis, Writing review & editing.

Declaration of competing interest

The authors declare that they have no known competing financial interests or personal relationships that could have appeared to influence the work reported in this paper.

Data availability

The authors are unable or have chosen not to specify which data has been used.

Acknowledgements

Financial support to complete this study was provided by the U.S. Department of Transportation, Office of the Assistant Secretary for Research and Technology (OST-R) under the Auspices of the INSPIRE University Transportation Center under Grant No. 69A3551747126 at Missouri University of Science and Technology.

References

[1] M. Raupach, P. Schiessl, Monitoring system for the penetration of chlorides, carbonation and the corrosion risk for the reinforcement, Constr. Build. Mater. 11 (4) (1997) 207–214, https://doi.org/10.1016/S0950-0618(97)00039-1.
[2] P. Ma, L. Fan, G. Chen, Hyperspectral reflectance for determination of steel rebar corrosion and Cl− concentration, Constr. Build. Mater. 368 (2023), 130506, https://doi.org/10.1016/j.conbuildmat.2023.130506.
[3] A. Ejbouh, A. Ech-chebab, S. Hassi, M. Galai, H. Benqlilou, M.E. Touhami, Durability assessment of LC3-based reinforced concrete under combined chloride-sulfate environment via the EIS technique, Constr. Build. Mater. 366 (2023), 130194, https://doi.org/10.1016/j.conbuildmat.2022.130195.
[4] P. Ma, J. Li, Y. Zhuo, P. Jiao, G. Chen, Coating condition detection and assessment on the steel girder of a bridge through hyperspectral imaging, Coatings 13 (6) (2023) 1008, https://doi.org/10.3390/coatings13061008.
[5] E.O. Fanijo, J.T. Kolawole, A. Almakrab, Alkali-silica reaction (ASR) in concrete structures: mechanisms, effects and evaluation test methods adopted in the United States, Case Stud. Construct. Mater. 15 (2021), e00563, https://doi.org/10.1016/j.cscm.2021.e00563.
[6] R.B. Figueira, R. Sousa, L. Coelho, M. Azenha, J.M. de Almeida, P.A.S. Jorge, C.J. R. Silva, Alkali-silica reaction in concrete: mechanisms, mitigation and test methods, Constr. Build. Mater. 222 (2019) 903–931, https://doi.org/10.1016/j.conbuildmat.2019.07.230.
[7] W. Wang, T. Noguchi, Alkali-silica reaction (ASR) in the alkali-activated cement (AAC) system: a state-of-the-art review, Constr. Build. Mater. 252 (2020), 119105, https://doi.org/10.1016/j.conbuildmat.2020.119105.
[8] F. Rajabipour, E. Giannini, C. Dunant, J.H. Ideker, M.D. Thomas, Alkali–silica reaction: current understanding of the reaction mechanisms and the knowledge gaps, Cem. Concr. Res. 76 (2015) 130–146, https://doi.org/10.1016/j.cemconres.2015.05.024.

[9] A. Gholizadeh-Vayghan, F. Rajabipour, The influence of alkali–silica reaction (ASR) gel composition on its hydrophilic properties and free swelling in contact with water vapor, Cem. Concr. Res. 94 (2017) 49–58, https://doi.org/10.1016/j.cemconres.2017.01.006.

[10] Z. Shi, G. Geng, A. Leemann, B. Lothenbach, Synthesis, characterization, and water uptake property of alkali-silica reaction products, Cem. Concr. Res. 121 (2019) 58–71, https://doi.org/10.1016/j.cemconres.2019.04.009.

[11] A.G. Vayghan, F. Rajabipour, J.L. Rosenberger, Composition–rheology relationships in alkali–silica reaction gels and the impact on the gel's deleterious behavior, Cem. Concr. Res. 83 (2016) 45–56, https://doi.org/10.1016/j.cemconres.2016.01.011.

[12] M. Pathirage, F. Bousikhane, M. D'ambrosia, M. Alnaggar, G. Cusatis, Effect of alkali silica reaction on the mechanical properties of aging mortar bars: experiments and numerical modeling, Int. J. Damage Mech. 28 (2) (2019) 291–322, doi:10.1177%2F1056789517750213.

[13] Z. Shi, B. Lothenbach, The combined effect of potassium, sodium and calcium on the formation of alkali-silica reaction products, Cem. Concr. Res. 127 (2020), 105914, https://doi.org/10.1016/j.cemconres.2019.105914.

[14] R. Tänzer, Y. Jin, D. Stephan, Effect of the inherent alkalis of alkali activated slag on the risk of alkali silica reaction, Cem. Concr. Res. 98 (2017) 82–90, https://doi.org/10.1016/j.cemconres.2017.04.009.

[15] A. Leemann, P. Lura, E-modulus of the alkali–silica-reaction product determined by micro-indentation, Constr. Build. Mater. 44 (2013) 221–227, https://doi.org/10.1016/j.conbuildmat.2013.03.018.

[16] W. Wang, T. Noguchi, I. Maruyama, Mechanism understanding of alkali-silica reaction in alkali-activated materials system, Cem. Concr. Res. 156 (2022), 106768, https://doi.org/10.1016/j.cemconres.2022.106768.

[17] T. Williamson, M.C. Juenger, The role of exposing solution concentration on alkali–silica reaction in alkali-activated fly ash concrete, Cem. Concr. Res. 83 (2016) 124–130, https://doi.org/10.1016/j.cemconres.2016.02.008.

[18] D. Bulteel, E. Garcia-Diaz, C. Vernet, H. Zanni, Alkali–silica reaction: a method to quantify the reaction degree, Cem. Concr. Res. 32 (8) (2002) 1199–1206, https://doi.org/10.1016/S0008-8846(02)00759-7.

[19] I. García-Lodeiro, A.Y. Palomo, A. Fernández-Jiménez, Alkali–aggregate reaction in activated fly ash systems, Cem. Concr. Res. 37 (2) (2007) 175–183, https://doi.org/10.1016/j.cemconres.2006.11.002.

[20] Z. Shi, B. Lothenbach, The role of calcium on the formation of alkali-silica reaction products, Cem. Concr. Res. 126 (2019), 105898, https://doi.org/10.1016/j.cemconres.2019.105898.

[21] J. Lei, W.W. Law, E.H. Yang, Effect of calcium hydroxide on the alkali-silica reaction of alkali-activated slag mortars activated by sodium hydroxide, Constr. Build. Mater. 272 (2021), 121868, https://doi.org/10.1016/j.conbuildmat.2020.121868.

[22] T. Kim, J. Olek, Chemical sequence and kinetics of alkali-silica reaction part I. Experiments, J. Am. Ceram. Soc. 97 (7) (2014) 2195–2203, https://doi.org/10.1111/jace.12992.

[23] T. Kim, J. Olek, Chemical sequence and kinetics of alkali–silica reaction part II. A thermodynamic model, J. Am. Ceram. Soc. 97 (7) (2014) 2204–2212, https://doi.org/10.1111/jace.12830.

[24] Z. Shi, A. Leemann, D. Rentsch, B. Lothenbach, Synthesis of alkali-silica reaction product structurally identical to that formed in field concrete, Mater. Des. 190 (2020), 108562, https://doi.org/10.1016/j.matdes.2020.108562.

[25] G. Geng, Z. Shi, A. Leemann, C. Borca, T. Huthwelker, K. Glazyrin, I.V. Pekov, S. Churakov, B. Lothenbach, R. Dähn, E. Wieland, Atomistic structure of alkali-silica reaction products refined from X-ray diffraction and micro X-ray absorption data, Cem. Concr. Res. 129 (2020), 105958, https://doi.org/10.1016/j.cemconres.2019.105958.

[26] Z. Li, R.J. Thomas, S. Peethamparan, Alkali-silica reactivity of alkali-activated concrete subjected to ASTM C 1293 and 1567 alkali-silica reactivity tests, Cem. Concr. Res. 123 (2019), 105796, https://doi.org/10.1016/j.cemconres.2019.105796.

[27] A. Leemann, Z. Shi, M. Wyrzykowski, F. Winnefeld, Moisture stability of crystalline alkali-silica reaction products formed in concrete exposed to natural environment, Mater. Des. 195 (2020), 109066, https://doi.org/10.1016/j.matdes.2020.109066.

[28] K.W. Liu, A.K. Mukhopadhyay, A kinetic-based ASR aggregate classification system, Constr. Build. Mater. 68 (2014) 525–534, https://doi.org/10.1016/j.conbuildmat.2014.07.005.

[29] K.M.D.V. Moreira, P.V.G. Oliveira, Ê.P. de Deus, A.E.B. Cabral, Alkali-silica reaction: understanding the phenomenon, J. Build. Pathol. Rehabil. 6 (1) (2021) 1–10, https://doi.org/10.1007/s41024-020-00100-3.

[30] F. Zhang, X. Yao, T. Yang, X. Gao, C. Geng, T. Jiang, Rheology and alkali-silica reaction of alkali-activated slag mortars modified by fly ash microsphere: a comparative analysis to OPC mortars, Mater. Res. Express 8 (6) (2021), 065501, https://doi.org/10.1088/2053-1591/ac03ee.

[31] M.H. Shehata, M.D. Thomas, The effect of fly ash composition on the expansion of concrete due to alkali–silica reaction, Cem. Concr. Res. 30 (7) (2000) 1063–1072, https://doi.org/10.1016/S0008-8846(00)00283-0.

[32] Z. Shi, C. Shi, S. Wan, N. Li, Z. Zhang, Effect of alkali dosage and silicate modulus on carbonation of alkali-activated slag mortars, Cem. Concr. Res. 113 (2018) 55–64, https://doi.org/10.1016/j.cemconres.2018.07.005.

[33] M. Khan, N. Newaz, P.K. Sarker, Alkali silica reaction of waste glass aggregate in alkali activated fly ash and GGBFS mortars, Mater. Struct. 52 (5) (2019) 1–17, https://doi.org/10.1617/s11527-019-1392-3.

[34] H. Du, K.H. Tan, Effect of particle size on alkali–silica reaction in recycled glass mortars, Constr. Build. Mater. 66 (2014) 275–285, https://doi.org/10.1016/j.conbuildmat.2014.05.092.

[35] C.F. Dunant, K.L. Scrivener, Effects of aggregate size on alkali–silica-reaction induced expansion, Cem. Concr. Res. 42 (6) (2012) 745–751, https://doi.org/10.1016/j.cemconres.2012.02.012.

[36] ASTM Standard C1260, 200“, "Standard Test Method for Potential Alkali Reactivity of Aggregates (Mortar-Bar Meth”d)", ASTM International, West Conshohocken, PA, 2021, https://doi.org/10.1520/C1260-21.

[37] X. Hou, R.J. Kirkpatrick, L.J. Struble, P.J. Monteiro, Structural investigations of alkali silicate gels, J. Am. Ceram. Soc. 88 (4) (2005) 943–949, https://doi.org/10.1111/j.1551-2916.2005.00145.x.

[38] H. Wu, J. Pan, J. Wang, Nano-scale structure and mechanical properties of ASR products under saturated and dry conditions, Sci. Rep. 10 (1) (2020) 1–9, https://doi.org/10.1038/s41598-020-66262-9.

[39] M. Shakoorioskooie, M. Griffa, A. Leemann, R. Zboray, P. Lura, Alkali-silica reaction products and cracks: X-ray micro-tomography-based analysis of their spatial-temporal evolution at a mesoscale, Cem. Concr. Res. 150 (2021), 106593, https://doi.org/10.1016/j.cemconres.2021.106593.

[40] R.J. Prado, F. Tiecher, N.P. Hasparyk, D.C.C. Dal Molin, Structural characterization of alkali-silica reaction gel: an x-ray absorption fine structure study, Cem. Concr. Res. 123 (2019), 105774, https://doi.org/10.1016/j.cemconres.2019.05.019.

[41] R. Dupuis, R.J. Pellenq, Alkali silica reaction: a view from the nanoscale, Cem. Concr. Res. 152 (2022), 106652, https://doi.org/10.1016/j.cemconres.2021.106652.

[42] Z. Shi, S. Park, B. Lothenbach, A. Leemann, Formation of shlykovite and ASR-P1 in concrete under accelerated alkali-silica reaction at 60 and 80 C, Cem. Concr. Res. 137 (2020), 106213, https://doi.org/10.1016/j.cemconres.2020.106213.

[43] A. Leemann, Raman microscopy of alkali-silica reaction (ASR) products formed in concrete, Cem. Concr. Res. 102 (2017) 41–47, https://doi.org/10.1016/j.cemconres.2017.08.014.

[44] C. Balachandran, J.F. Muñoz, T. Arnold, Characterization of alkali silica reaction gels using Raman spectroscopy, Cem. Concr. Res. 92 (2017) 66–74, https://doi.org/10.1016/j.cemconres.2016.11.018.

[45] T.C. Ling, C. Balachandran, J.F. Munoz, J. Youtcheff, Chemical evolution of alkali–silicate reaction (ASR) products: a Raman spectroscopic investigation, Mater. Struct. 51 (2018) 1–9, https://doi.org/10.1617/s11527-018-1151-x.

[46] C.M. Strack, T.L. Thornell, J.A. Jefcoat, G.J. Borne, P. Alapati, K.E. Kurtis, R. D. Moser, The viscoelastic behavior of synthetic alkali-silica gels at ambient temperature, Cem. Concr. Res. 165 (2023), 107069, https://doi.org/10.1016/j.cemconres.2022.107069.

[47] A. Leemann, B. Münch, The addition of caesium to concrete with alkali-silica reaction: implications on product identification and recognition of the reaction sequence, Cem. Concr. Res. 120 (2019) 27–35, https://doi.org/10.1016/j.cemconres.2019.03.016.

[48] A. Gholizadeh-Vayghan, F. Rajabipour, Quantifying the swelling properties of alkali-silica reaction (ASR) gels as a function of their composition, J. Am. Ceram. Soc. 100 (8) (2017) 3801–3818, https://doi.org/10.1111/jace.14893.

[49] A.G. Vayghan, F. Rajabipour, J.L. Rosenberger, Composition–rheology relationships in alkali–silica reaction gels and the impact on the gel's deleterious behavior, Cem. Concr. Res. 83 (2016) 45–56, https://doi.org/10.1016/j.cemconres.2016.01.011.

[50] I. Maruyama, G. Igarashi, Y. Nishioka, Bimodal behavior of CSH interpreted from short-term length change and water vapor sorption isotherms of hardened cement paste, Cem. Concr. Res. 73 (2015) 158–168, https://doi.org/10.1016/j.cemconres.2015.03.010.